

Optimum Conditions for the Catalytic Cracking of Palm Oil from Empty Fruit Bunch over Dolomite in a Continuous Reactor

Phasatorn Khunoad¹, Phorndranrat Suchamalawong², Kittiphop Promdee^{3,5*}, and Tharapong Vitidsant^{4,5*}

¹ Program for Petrochemical and Polymer Science, Faculty of Science, Chulalongkorn University, Bangkok, 10330, Thailand

² Interdisciplinary Program of Environmental Science, Graduate School, Chulalongkorn University, Bangkok, 10330, Thailand

³ Department of Environmental Science, Academic Division, Chulachomklao Royal Military Academy, Nakhon Nayok, 26001, Thailand

⁴ Department of Chemical Technology, Faculty of Science, Chulalongkorn University, Bangkok 10330, Thailand^f

⁵ Center of Fuels and Energy from Biomass, Chulalongkorn University, Saraburi 18110, Thailand

Received May 18, 2020; Accepted September 21, 2020

Abstract

This research evaluates the effectiveness of cracking palm oil from an empty fruit bunch (EFB) over dolomite in a continuous reactor and used the 2k factorial design to investigate the influence of parameters, such as reaction temperature (380-460°C), feed rate of palm oil (3-9 mL/min), nitrogen gas flow rate (50-150 mL/min), and the amount of catalyst (30-60% by reactor volume) that affected the yield of organic liquid product (OLP) and diesel-like fraction. OLP was obtained and analyzed by using distillation simulation gas chromatography and gas chromatograph mass-spectrometry to identify the structure of liquid fuels. An analysis from the design-expert program demonstrated that the optimum conditions for the catalytic cracking of PEFB on dolomite in continuous reactor were: a temperature of 460°C, feed rate of palm oil 8.96 mL/min, nitrogen gas flow rate of 50.04 mL/min, and the amount of catalyst 60% (v/v), which yielded the highest diesel-like fraction of 66.12%wt and a liquid yield of 57.93%wt. The physicochemical analysis of OLP resulted in a heating value of 45.20 MJ/kg and acidity value of 0.35 mgKOH/g.

Keywords: Catalytic cracking; Empty fruit bunch (PEFB); Dolomite; Organic liquid product (OLP).

1. Introduction

Biodiesel is bio-renewable and environmentally-friendly fuel that can be made from triglyceride in animal fats or vegetable oils by a trans-esterification reaction with alcohols, such as methanol and ethanol, using a homogeneous base or acid catalysts [1-7]. Nevertheless, these systems of homogeneous catalysis have many disadvantages since a purification process is required to remove these catalysts from the end products. In this regard, glycerol as a by-product has proven to be difficult to remove and requires an immense amount of water to do so. Therefore, the catalytic cracking of triglycerides represents an alternative way to produce biofuel with fewer complications and less use of resources. In addition, the process also has lower production costs, lower equipment costs, and compatibility with existing infrastructure and feed stock flexibility [8-11], which result in final products that have a composition similar to diesel fuel [12-15].

With regard to the raw materials used in this research, the empty fruit bunch (EFB) is a commonly available biomass waste residue generated from the palm oil industries in Thailand and other locations, particularly in Southeast Asia [16-19]. The EFBs are often incinerated at the plant site, which causes air pollution. The successful conversion of these waste materials to

produce biofuels may, therefore, provide environmental, as well as additional financial benefits. Dolomite ($\text{CaMg}(\text{CO}_3)_2$) is a mineral that consists of calcium carbonate and magnesium carbonate, which has low toxicity, low cost, and high basicity. It is a naturally abundant mineral in many areas of Thailand. Currently, this mineral is mostly used for cement manufacturing and landfill due to its low cost, low toxicity, high basicity, and environmentally-friendly properties. The material was chosen for this experiment in light of the extent of its successful application in biodiesel production, as reflected in numerous existing literature [20].

The objective of this research was to investigate the optimum conditions for the production of biofuel through the catalytic cracking of palm oil from empty fruit bunches (EFB) on dolomite in continuous reactor. The experiments were designed to study the effect of different types of catalysts and other factors such as the reaction temperature, feed rate, nitrogen gas flow rate, and the amount of catalysts on the liquid yield and diesel fraction from obtained biofuel.

2. Methodology

2.1. EFB preparation and characterization

The EFB used in this study as the feedstock was obtained from Southern Palm (1978) Company Limited in Thailand. The palm oil sample was filtered through filter paper to remove solid impurities and was heated to 100-110°C for 10 minutes to remove moisture prior to its use in cracking. The thermal decomposition of sample was evaluated by thermo-gravimetric analysis (TGA) carried out by a Setaram LABSYS EVO thermogravimeter at a ramping rate of 20°C/min in an argon atmosphere.

2.2. Catalyst preparation and characterization

The dolomite, which will be the experiment's catalyst, was obtained from L S M (1999) Company Limited in Thailand. The dolomite was dried in the oven at 110°C for 2 hours to remove all surface moisture and calcined at 600°C for 1 hour in a muffle furnace to remove impurities and left to cool to room temperature.

The X-ray diffraction (XRD) was performed by a Bruker AXS D8 Discover. The samples were scanned from 5 to 70°. The diffractograms were analyzed using the standard JCPDS files. Elemental analysis was performed by an AXIOS PW-4400 fluorescence spectrometer. Morphological study was carried out by a JOEL JSM-5800LV scanning electron microscope. The instrument was operated at 15 kV acceleration voltages. Prior to analysis, samples were coated with a thin film of gold to make them conductive. The N_2 adsorption and desorption isotherms were measured by a Micromeritics ASAP 2020 instrument. Pore size distributions of the samples were determined from the isotherms by the Barrett-Joyner-Hallenda (BJH) method. All samples were dried in the oven at 110°C overnight before the adsorption measurement.

2.3. Catalytic cracking reaction

The cracking of palm oil from EFB was conducted in a continuous reactor 3 L (Biodiesel reactor unit, model no. Bio-3401) from HIRO Company Limited in Japan. The dolomite as catalyst was loaded over quartz wool and placed in the horizontal furnace. The temperature was monitored by a thermocouple positioned in the center of catalyst bed. Nitrogen gas as a carrier gas was passed through the reactor throughout the reaction. The reaction temperature was in the range of 380 to 460°C. The palm oil was fed using a rotary pump (Iwaki Metering Pump model no. LK-22VSH-02). Once a stable state was reached in the reactor, the liquid product (organic and aqueous fractions) was collected in a liquid sampler, while the gaseous products were collected in a gas-sampling tube. The process run time for each experiment was 5 hours.

The gaseous product was analyzed using column (Molecular sieve packed columns) over gas chromatograph (Agilent 7820A), equipped with thermal conductivity detector (TCD). The OLP was analyzed by gas chromatograph simulated distillation (GC SimDist) using a capillary glass column (100% dimethylpolysiloxane stationary phase, J&W Scientific, DB-HT-SIMDIS, 5 m length \times 0.53 mm diameter \times 0.15 μm film thickness) over gas chromatograph (Agilent

7890A), equipped with flame ionization detector (FID). The OLP contains a large number of components of hydrocarbon compounds.

Consequently, the composition of liquid product was defined according to the boiling range of petroleum products in three categories, that is gasoline fraction (273.15-473.15 K), kerosene fraction (473.15-523.15 K), and diesel fraction (523.15-643.15 K). The liquid product identification and composition determination were performed on a GC Agilent series 7890A with a Agilent mass selective detector of series 5975C using a capillary glass column (J&W Scientific, 100% dimethylpolysiloxane stationary phase, HP-5MS, 30 m length × 0.25 mm diameter × 0.25 μm film thickness). The yield of organic liquid products was calculated using the following equation:

$$\text{Yield (wt\%)} = \left(\frac{\text{Obtained Product(g)}}{\text{PEFB Feed(g)}} \right) \times 100\% \quad (1)$$

2.4. 2⁴ Factorials design

Table 1. 2⁴ factorials design containing five central points

Run	Code factors			
	A	B	C	D
1	-1	-1	-1	-1
2	+1	-1	-1	-1
3	-1	+1	-1	-1
4	+1	9	-1	-1
5	-1	3	+1	-1
6	+1	3	+1	-1
7	-1	9	+1	-1
8	+1	9	+1	-1
9	-1	3	50	+1
10	+1	3	50	+1
11	-1	9	50	+1
12	+1	9	50	+1
13	-1	3	+1	+1
14	+1	3	+1	+1
15	-1	9	+1	+1
16	+1	9	+1	+1
17	0	0	0	0
18	0	0	0	0
19	0	0	0	0
20	0	0	0	0
21	0	0	0	0

3. Results and discussion

3.1. Oil characterization

The fatty acid composition was determined by gas chromatography simulation distribution (standard method D2887). The analysis of the EFB's boiling point before catalytic cracking was determined by DGC standard ASTM D2887, as shown in Table 2. The EFB was mainly composed of long residue at 84.50% whereas the quantity of diesel was 15.50%. The EFB cannot be directly used in engines and requires further processing to improve its quality. The catalytic pyrolysis process breaks down the large molecules to smaller hydrocarbon molecules. The OLP created from pyrolysis has similar properties to generic diesel oil and benzene oil, as well as other physical and chemical properties that are similar to petroleum diesel oil.

The composition of the EFB was determined in the terms of different types of fatty acids as represented in Table 3. The result showed that the majority proportion (43.07%) of palmitic acid (C16:0) was saturated, while 39.72% oleic acid (C18:1) was an unsaturated fatty acid.

Table 2. The distribution of palm oil from empty fruit bunch, as analyzed by gas chromatography simulation distribution (DGC)

Boiling point	Composition	Recovery (wt%)
IBP-200	Naphtha (C ₅ -C ₁₂)	0.00
200-250	Kerosene(C ₁₂ -C ₁₅)	0.00
250-370	Diesel(C ₁₅ -C ₃₃)	15.50
370-FBP	Long residue(>C ₃₃)	84.50

Table 3. Composition of fatty acid of EFB

Fatty acid composition, g/100 g		
Lauric acid	C12:0	0.30
Myristic acid	C14:0	0.90
Pentadecanoic acid	C15:0	0.05
Palmitic acid	C16:0	43.07
Hepadecanoic acid	C17:0	0.12
Stearic acid	C18:0	4.38
Arachidic acid	C20:0	0.36
Behenic acid	C22:0	0.08
Lignoceric acid	C24:0	0.10
Total saturated fatty acid		49.36
Palmitoleic acid	C16:1	0.15
Oleic acid	C18:1	39.72
Cis-9, 12-Octadecadienoic acid	C18:2	9.96
Cis-9, 12, 15-Octadecatrienoic acid	C18:3	0.31
Cis-11-Eicosenoic acid	C20:1	0.14
Nervonic acid	C24:1	0.14
Total unsaturated fatty acid		50.42
Unidentified peak		0.24

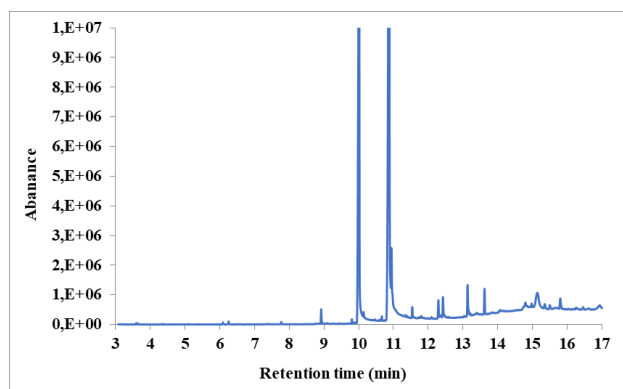


Figure 1 GC-MS Chromatograms of palm oil from EFB

The chemical compound of the EFB was analyzed by gas chromatograph-mass spectrometry. Figure 1, shows the chromatogram of the EFB sample. For the purpose of clarity, the solvent peaks (carbon disulfide) are not shown. The n-hexadecanoic acid (palmitic acid, C₁₆:0) appears at a retention time of 10.015 min, followed by 9-Octadecenoic acid (oleic acid, C₁₈:1), which appeared at a retention time of 10.879 min and octadecanoic acid (stearic acid, C₁₈:0) peak appears at a retention time of 10.946 min, as shown in Table. 4. The large peaks of GC-MS chromatogram, mostly shows carboxylic acid, while small peaks show other groups. The EFB is a source of hydrocarbons C₁₆-C₁₈ atoms, which is similar to the number of carbon atoms of diesel produced from petroleum distillation.

A thermal analysis of the EFB's decomposition temperature was also performed. The TGA curves of the EFB are shown in Figure 2 and demonstrate the fact that the EFB begins to thermally decompose at approximately 155°C, while the high temperature of decomposition is 440°C, at a heating rate of 20°C/min from 25 to 600°C, under the inert gas (argon) atmosphere. Consequently, the decomposition temperature range of 380 to 460°C was chosen for the cracking of the EFB.

Table 4. The chemical compound of EFB

Retention time (min)	Name	Formula chemical	Area (%)
10.015	n-Hexadecanoic acid	C ₁₆ H ₃₂ O ₂	34.88
10.145	Octadecanoic acid	C ₁₈ H ₃₄ O ₂	0.98
10.877	6-Octadecenoic acid	C ₁₈ H ₃₄ O ₂	48.15
10.947	Octadecanoic acid	C ₁₈ H ₃₄ O ₂	6.33
12.291	9-Octadecenal, (Z)-	C ₁₈ H ₃₄ O	0.79
13.617	Squalene	C ₃₀ H ₅₀	0.90
14.792	Benzo[h]quinoline, 2,4-dimethyl-	C ₁₅ H ₁₃ N	0.92
15.135	Cyclotrisiloxane, hexamethyl-	C ₆ H ₁₈ O ₃ Si ₃	3.95
15.798	2-Ethylacridine	C ₁₅ H ₁₃ N	0.67

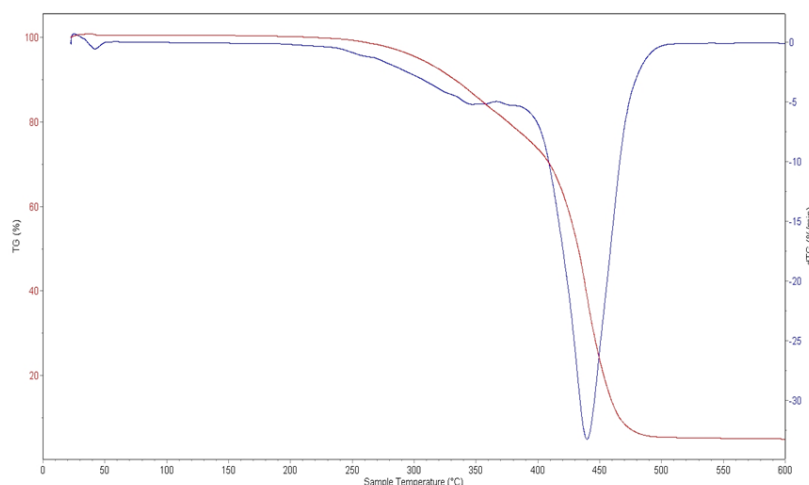


Figure 2 Thermal decomposition analysis of PEFB by thermogravimetric analyzer

3.2. Catalyst characterization

3.2.1. X-ray Fluorescence (XRF)

The catalyst used in this study was powdered dolomite. Its chemical composition, as determined through X-ray fluorescence (XRF) analysis, is as follows: CaO 59.80%, MgO 33.5%, SiO₂ 0.39%, Fe₂O₃ 0.23%, Al₂O₃ 0.19% and Others 5.89%. The XRF analysis result can be seen in Table 5. It is observed that the CaO content in the dolomite is higher than MgO content. Calculations by stoichiometry on the XRF analysis showed that the dolomite consisted of 59.80 wt% CaO and MgO 33.50 wt%.

Table 5. Chemical composition of dolomite

Compound	Concentration (wt%)
Calcium (CaO)	59.80
Magnesium (MgO)	33.50
Silica (SiO ₂)	0.39
Iron (Fe ₂ O ₃)	0.23
Aluminium (Al ₂ O ₃)	0.19
Other	5.89

3.2.2. X-ray powder diffraction (XPD)

Figure 3 shows the X-ray Powder Diffraction (XPD) patterns of the raw dolomite and calcined dolomite at 800°C. It can be seen that CaO, MgO, Mg(OH)₂ and Ca(OH)₂ is present in the raw dolomite. A decarbonation occurs with the increase in calcination temperature, which leads to the transformation of CaMg(CO₃)₂ to CaO, MgO and carbonate phase of CaCO₃ or calcite. The diffraction peak intensities of MgO increased relatively after calcination and the

peak of calcium hydroxide ($\text{Ca}(\text{OH})_2$) and magnesium hydroxide ($\text{Mg}(\text{OH})_2$) disappears in an XPD analysis of calcined dolomite.

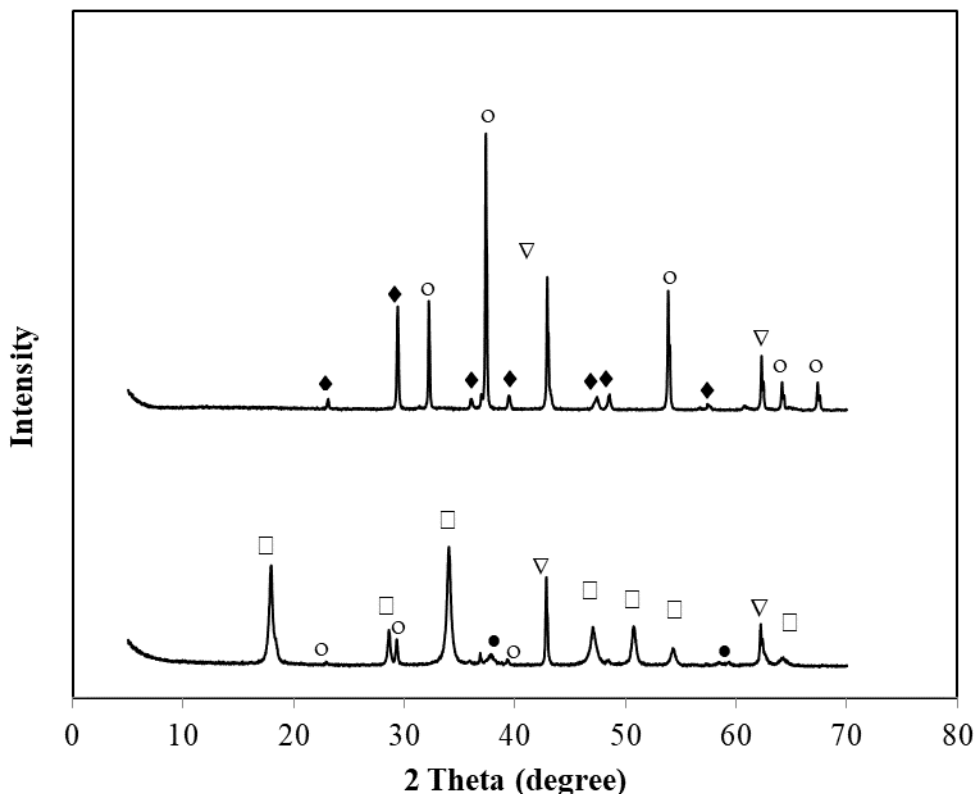


Figure 3. XPD pattern of dolomite (a) raw dolomite and (b) calcined dolomite at 800°C , symbol: (●) $\text{Mg}(\text{OH})_2$, (□) $\text{Ca}(\text{OH})_2$, (◆) CaCO_3 , (▽) MgO , and (○) CaO

3.2.3. BET surface area measurement

The surface areas of the raw dolomite and calcined dolomite were determined through the nitrogen adsorption method and the BET equation, as shown in Table 6. The maximum activity was obtained with the catalyst calcined at 800°C for 2 hours. Table 6 shows the specific surface area and porosity of the dolomite. Decarbonation by the calcination of the dolomite produces MgO and increases its specific surface area. Thus, the BET surface area of raw dolomite $8.00 \text{ m}^2\text{g}^{-1}$ was significantly increased to $19.95 \text{ m}^2\text{g}^{-1}$ after thermal treatment at 800°C . The dolomite also saw increases in pore volume and diameter.

The thermal decomposition of dolomite occurs via a system involving a number of reactions that are still being debated in existing literature. When performed in vacuum or in an inert atmosphere, this is also a one-step reaction leading to the mixture of magnesium or calcium oxides. When it takes place in air or in the presence of CO_2 , it occurs as a two-step process. Thus, the phenomenon that occurs during the thermal decomposition of fresh dolomite can be expressed as follows:

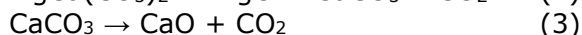
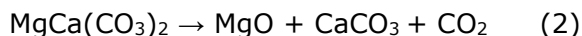


Table 6. Specific surface area and porosity of examined dolomite

Sample	Specific surface area ($\text{m}^2 \text{g}^{-1}$)	Total pore volume ($\text{cm}^3 \text{g}^{-1}$)
Raw dolomite	8.00	0.01
Calcined dolomite	19.95	0.10

3.2.4. SEM analysis

The results of the SEM analysis is shown in Figure 4. Changes in the morphology of the dolomite were observed as a result of recrystallization when undergoing calcination. The SEM image of the raw dolomite clearly shows that it had a wide range of particles sizes in random shapes and may display a macropore or almost non-porous structure. The microstructure of calcined dolomite has a porous surface, the particle size decreased due to cracking large particles from the decarbonation of dolomite (chemical equation 1-2). This phenomenon is caused by the release of CO₂ from the dolomite grain and it proves that the dolomite calcinations reaction originated on the surface of dolomite.

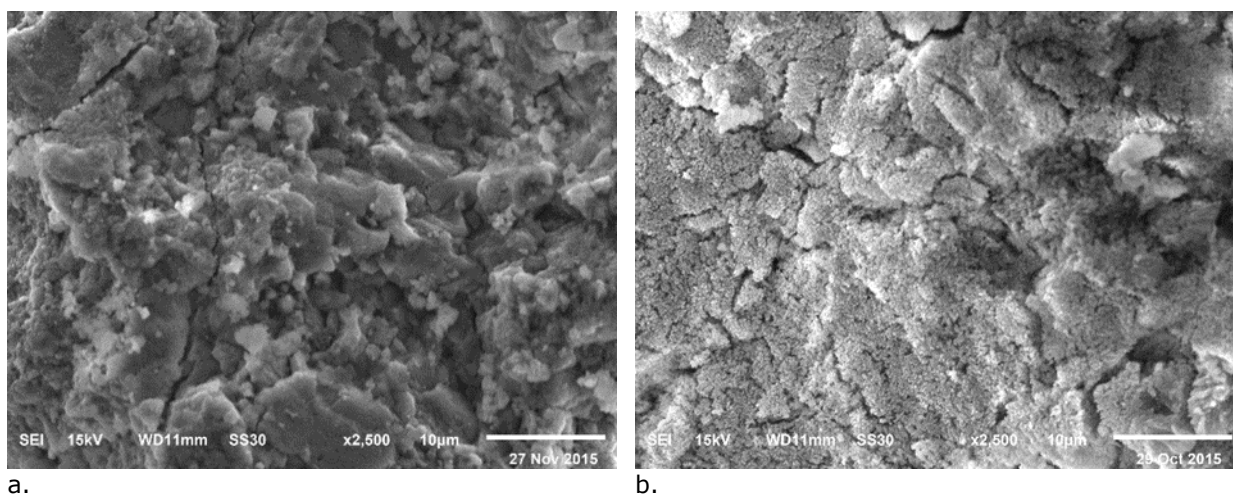


Figure 4. Electron micrograph of raw dolomite (a) and calcined dolomite (b) at 2500x magnification

3.3. Yield liquid

Table 8 shows the highest yield of liquid and diesel-like fuel that can be obtained from the catalytic cracking of palm oil from the EFB. The important operating variables affecting the liquid yield and product distribution were: reaction temperature, feed rate, flow rate of the carrier gas, and the amount of catalyst. A 2^k factorial design with three process variables where each containing three levels, namely low (-1), central (0), and high level (+1) was used. Table 7 presents the 2^k full factorial design with the operating range of each variable. The total number of experiments conducted was 16, where five experiments were repeated at the central level of each factor to check their reproducibility and experimental error.

The results show that higher temperatures and lower feed rates gave higher yields of gaseous product, while low reaction temperatures and high feed rate deactivated the catalyst [21-29]. The conversion of EFB, yield of OLP and yield of diesel-like fraction at different reaction are presented in Table 8. It shows that the OLP varied in the range of from 7.08 to 65.76 wt%. The OLP increased steadily with the increase in the reaction temperature due to higher cracking rates. The diesel-like fraction varied in the range of 47.50 to 74.35 wt%.

Table 7. Code factor and factor level of variable of cracking of palm oil from empty fruit bunch on dolomite in continuous reactor

Factor	Factor code	Level			Unit
		Low (-1)	Central point (0)	High (+1)	
Reaction temperature	A	380	420	460	°C
Feed rate of palm oil	B	3	6	9	mL/min
Flow rate of carrier gas (N ₂)	C	50	100	150	mL/min
The amount of catalyst	D	30	45	60	%v/v of reactor volume

Table 8. Experimental matrix and response obtained based on Design of Experiment

Run	Code factors				OLP yield (wt%)	Diesel fraction yield (wt%)
	A	B	C	D		
1	-1	-1	-1	-1	36.25	63.13
2	+1	-1	-1	-1	63.70	59.07
3	-1	+1	-1	-1	42.29	58.38
4	+1	9	-1	-1	65.76	56.25
5	-1	3	+1	-1	34.36	59.50
6	+1	3	+1	-1	55.58	57.82
7	-1	9	+1	-1	36.55	51.25
8	+1	9	+1	-1	63.14	47.50
9	-1	3	50	+1	28.20	74.35
10	+1	3	50	+1	53.84	67.81
11	-1	9	50	+1	30.40	71.88
12	+1	9	50	+1	61.68	66.13
13	-1	3	+1	+1	26.87	70.63
14	+1	3	+1	+1	51.62	63.44
15	-1	9	+1	+1	7.08	61.57
16	+1	9	+1	+1	59.19	62.25
Repeated trial						
17	0	0	0	0	42.87	49.38
18	0	0	0	0	37.01	48.75
19	0	0	0	0	39.69	49.13
20	0	0	0	0	33.79	50.62
21	0	0	0	0	40.86	48.73

3.4 Results of 2^k factorial design

3.4.1. Variables affecting the percentage of oil yield

To confirm the significance of variables on the percentage of oil yield, the 2^k factorials design was used to determine the effect of four operating parameters: reaction temperature (A), flow rate of oil (B), flow rate of carrier gas (C) and the amount of catalyst (%v/v) of reactor volume (D). The variables' significance was assessed using an analysis of variance (ANOVA).

Since several variables were studied, the conditions that significantly affected the product distribution had to be identified statistically. Figure 5 shows the half normal plot of the effect of reaction temperature (A), flow rate of oil (B), flow rate of carrier gas (C) and the amount of catalyst (%v/v) of reactor volume (D) were significant variables for OLP. Therefore, the ANOVA, was performed at 95% level of confidence for designed experiments using the Design-Expert software (version 6.0.6). The value of Prob > F for the models is less than 0.05, indicating that the model is significant and shows that the terms in the model has a significant effect on the response.

Table 9 shows the summary of the results obtained. It found that the reaction temperature (A), flow rate of oil (B), flow rate of carrier gas (C) and the amount of catalyst (%v/v) of reactor volume (D) have a value Prob > F less than 0.05 and implies that these variables affect the yield of OLP. Figure 6 shows the normal plot of residuals of OLP, the correlation coefficient for the OLP was 0.96. The data on OLP yield fits the normal distribution and contains no outliers.

Table 9. ANOVA result for the 2k factorials design of OLP

Source	Sum of Squares	Degree of freedom	Mean Square	F value	Prob > F value
Model	6160.75	4	1540.19	248.70	<0.0001
A	5504.37	1	5504.37	888.82	<0.0001
B	182.84	1	182.84	29.52	<0.0001
C	79.10	1	79.10	12.77	<0.0012
D	394.45	1	394.45	63.69	<0.0001
Residual	191.98	31	6.19		
Total	6586.43	36			

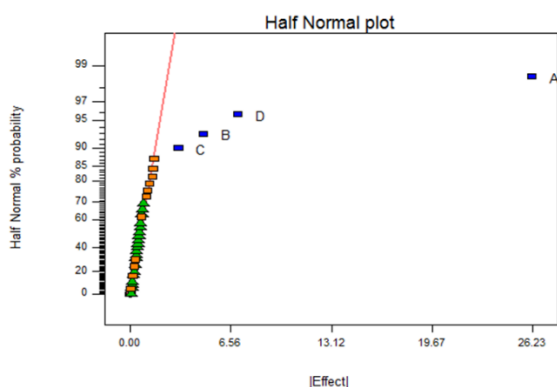


Figure 5. Half Normal probability plot of percentages yield of OLP

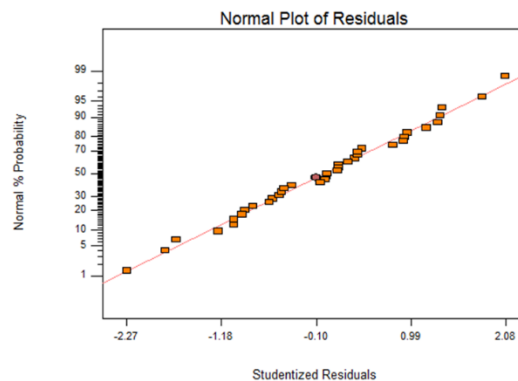


Figure 6. Normal probability plot versus studentized residuals of OLP

3.4.2. Variables affecting the percentage of diesel-like fraction yield

Figure 7 shows a half normal probability plot of the effect of reaction temperature (A), flow rate of oil (B), flow rate of carrier gas (C), the amount of catalyst (%v/v) of reactor volume (D), reaction temperature-the amount of catalyst (%v/v) of reactor volume of reaction interaction (AD), flow rate of oil-flow rate of carrier gas of reaction interaction (BC), and reaction temperature-flow rate of carrier gas-the amount of catalyst (%v/v) of reactor volume (ACD). It indicates that these variables are factors that affect the percentage yield of diesel products.

Table 10 shows the ANOVA results, which found that the reaction temperature (A), flow rate of oil (B), flow rate of carrier gas (C), the amount of catalyst (%v/v) of reactor volume (D), reaction temperature-the amount of catalyst (%v/v) of reactor volume of reaction interaction (AD), flow rate of oil-flow rate of carrier gas of reaction interaction (BC), and reaction temperature-flow rate of carrier gas-the amount of catalyst (%v/v) of reactor volume of reaction interaction (ACD) have a value Prob>F less than 0.05 percent and implies that these variables affect the yield of diesel products.

Figure 8 shows the normal plot of residues. The obtained data on diesel product was tested for normalcy to determine if the data obtained from the experiment is suitable for further statistical evaluation. It was determined that the percentage of diesel is approximately a straight line with $R^2 = 0.97$ and data on diesel product fit the normal distribution, while containing no outliers.

Table 10. ANOVA result for the 2k factorials design of diesel fraction

Source	Sum of Squares	Degree of freedom	Mean Square	F value	Prob > F value
Model	1608.63	7	229.80	164.18	<0.0001
A	92.24	1	92.24	65.90	<0.0001
B	180.83	1	180.83	129.19	<0.0001
C	201.55	1	201.55	143.99	<0.0001
D	1027.29	1	1027.29	733.91	<0.0001
AD	5.96	1	5.96	4.26	0.0485
BC	74.82	1	74.82	53.45	<0.0001
ACD	25.94	1	25.94	18.53	0.0002
Residual	39.19	28	1.40		
Total	2201.09	36			

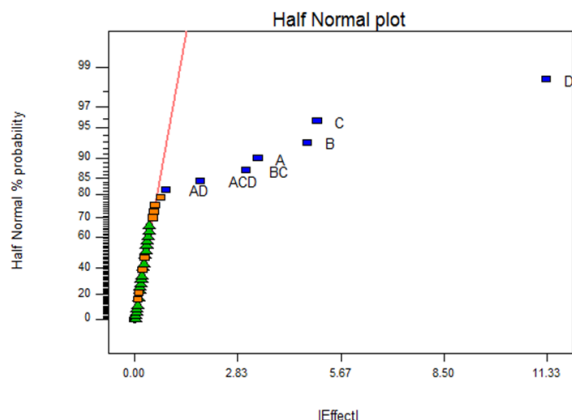


Figure 7. Half Normal probability plot of percent-ages yield of diesel-like fraction from the cracking of EFB on dolomite in continuous reactor

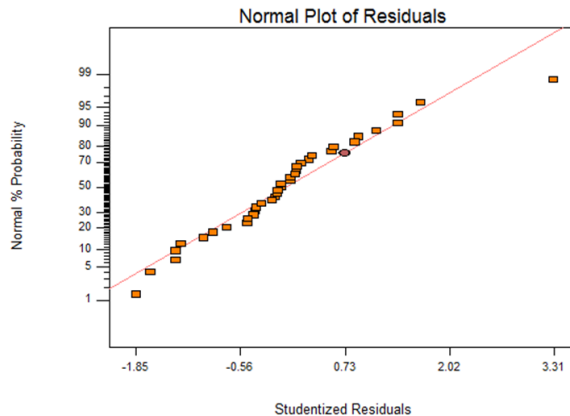


Figure 8. Normal probability plot versus studentized residuals of diesel fraction

3.5. Optimum conditions according to the Design-Expert 6.0.10 program

Table 11 shows an analysis from Design-Expert 6.0.10 program. According to the program, the optimum condition for catalytic cracking of palm oil from EFB on dolomite in continuous reactor is as follows: a temperature of 460°C, feed rate of palm oil 8.96 mL/min, nitrogen gas flow rate of 50.04 mL/min, and the amount of catalyst 60% (v/v). This gave the highest diesel-like fraction of 66.12%wt, whereas liquid yield was 57.93%wt. The desired criteria are summarized in Table 12, which shows that the values obtained from program and experiment yielded the same optimum condition.

Table 11. Optimization criteria

Name	Goal	Lower Limit	Upper Limit	Unit
Temperature	is in range	380	460	°C
Feed rate of palm oil	is in range	3	9	mL/min
Flow rate of carrier gas	is in range	50	150	mL/min
Catalyst	is in range	30	60	%v/v
Liquid yield	maximize	25.95	66.75	%wt
Diesel yield	maximize	47.5	75.57	%wt

Table 12. Optimum conditions from Design-Expert Program

Factor	Condition from program	Condition from experiment
Reaction temperature (°C)	460.00	460.00
Feed rate of palm oil (mL/min)	8.96	9.00
Flow rate of carrier gas (mL/min)	50.04	50.00
The amount of catalyst (v/v% reactor volume)	60.00	60.00
OLP (wt%)	59.73	61.68
Diesel fraction (wt%)	66.12	66.13

3.6. Properties of the biofuel

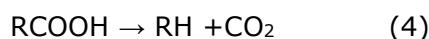
The elemental composition of the palm oil from the EFB (PEFB) and pyrolysis oils from triglyceride materials both with and without the dolomite are shown in Table 13. The analysis of the PEFB found that the following elemental contents: carbon, hydrogen, nitrogen, and oxygen (by reference) were 59.30, 12.00, 0.04 and 28.66% respectively. The analysis of the OLP shows that the carbon, hydrogen, nitrogen and oxygen (by reference) were 76.50, 12.80, 0.03 and 10.67% respectively. The presence of oxygen in OLP is lower than that of the oils from the PEFB. The decreasing of percentage of oxygen corresponded to the increase of the

heating value [30-34]. Normally, the effect of decreasing percentage of oxygen is that the heating value increases.

Table 13. Elemental analysis of the bio-oil

Oil	C	H	N	O*
PEFB	59.30	12.00	0.04	28.66
Non-catalyst	70.90	11.90	0.09	17.11
OLP	76.50	12.80	0.03	10.67

The total acid and heating value of PEFB and OLP were measured by potentiometric titration (ASTM D664), as shown in Table 14. The acid value of OLP is lower than the PEFB, decreasing from 54.44 to 0.35 mgKOH/g. The acid value was quite low when the catalyst contained MgO. These phenomena of decarboxylation of fatty acids to hydrocarbons were catalyzed by MgO, as shown in Equation 4 [1].



The heating value was determined for the catalytic cracking products and presented in Table 14. The heating value of OLP is higher than PEFB, increasing from 39.25 to 45.20 MJ/kg. It was observed that the OLP has characteristics similar to those of petroleum fuels.

Table 14. Acid and heating values of OLP

Oil	Acid value (mgKOH/g)	Heating value (MJ/kg)
PEFB	54.44	39.25
OLP	0.35	45.20

The chemical composition of OLP produced at optimum operating condition was analyzed by gas chromatograph-mass spectrometry and presented in Figure 9. The OLP produced can be classified into hydrocarbons, alcohols, phenol, esters, aldehydes, ketones, carboxylic acids, and other ester. GC MS analysis matches each peak observed in the chromatogram with a substance peak stored in the reference library. The result of the analysis is presented in Table 15. The GC-MS chromatograms large peaks mostly show aromatic, aliphatic and cyclic hydrocarbons while small peaks shows other groups.

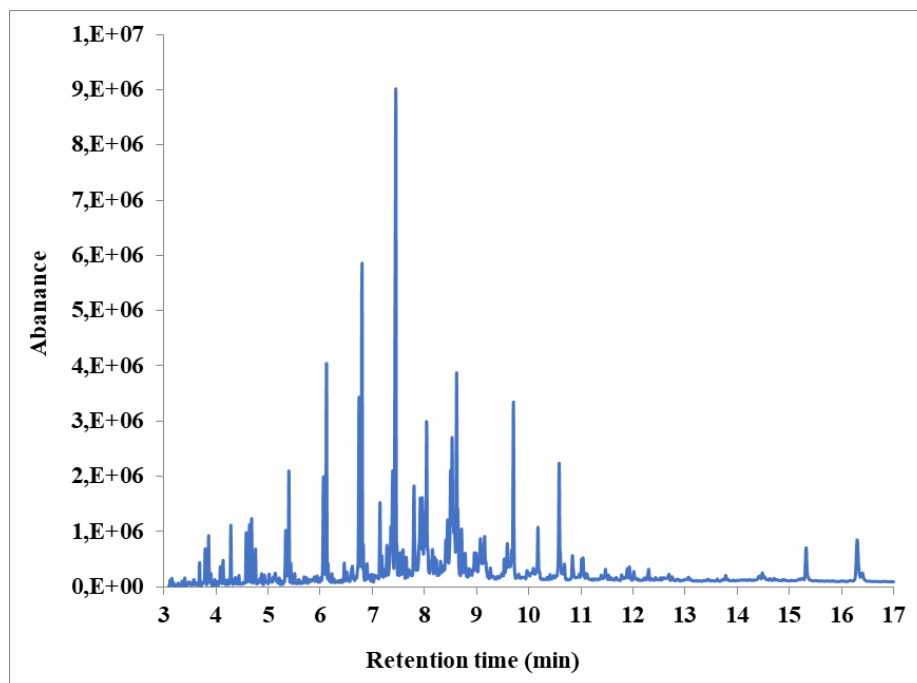


Figure 9. GC-MS Chromatograms of OLP

Table 15. The chemical compound in the oil yield product of cracking of PEFB on dolomite in continuous reactor

Time (min)	Name	Formula chemical	Area (%)
3.117	3-Nonene	C ₉ H ₁₈	0.06
3.147	2-Cyclopenten-1-one, 2-methyl-	C ₆ H ₈ O	0.09
3.182	cis-2-Nonene	C ₉ H ₁₈	0.04
3.269	Bicyclo[2.2.2]octane, 2-methyl-	C ₉ H ₁₆	0.05
3.343	Cyclohexane, propyl-	C ₉ H ₁₈	0.06
3.399	2-Cyclopenten-1-one, 3,4-dimethyl-	C ₇ H ₁₀ O	0.10
3.468	Cyclopentene, 1-butyl-	C ₉ H ₁₆	0.07
3.490	Cyclohexanone, 2-methyl-	C ₇ H ₁₂ O	0.08
3.568	Cyclohexene, 1-propyl-	C ₉ H ₁₆	0.09
3.681	Phenol	C ₆ H ₅ OH	0.28
3.763	2,4-Hexadienoic acid, ethyl ester (Ethyl sorbate)	C ₈ H ₁₂ O ₂	0.11
3.789	1-Decene	C ₁₀ H ₂₀	0.43
3.854	Decane	C ₁₀ H ₂₂	0.67
3.897	4-Decene	C ₁₀ H ₂₀	0.13
3.971	2-Decene, (Z)-	C ₁₀ H ₂₀	0.09
4.019	1-Tridecyne	C ₁₃ H ₂₄	0.05
4.132	D-Limonene	C ₁₀ H ₁₆	0.35
4.210	2-Cyclopenten-1-one, 2,3-dimethyl-	C ₇ H ₁₀ O	0.10
4.279	Phenol, 2-methyl-	C ₇ H ₈ O	0.73
4.348	Benzene, butyl-	C ₁₀ H ₁₄	0.08
4.435	Phenol, 3-methyl-	C ₇ H ₈ O	0.13
4.530	Cyclooctane, methyl-	C ₉ H ₁₈	0.09
4.578	1-Undecene	C ₁₁ H ₂₂	0.70
4.639	Undecane	C ₁₁ H ₂₄	0.85
4.678	5-Undecene	C ₁₁ H ₂₂	0.76
4.730	Phenol, 2,6-dimethyl-	C ₈ H ₁₀ O	0.14
4.752	5-Undecene	C ₁₁ H ₂₂	0.44
4.838	Cyclodecene, (Z)-	C ₁₀ H ₁₈	0.18
4.873	Cyclopentene, 1-butyl-	C ₉ H ₁₆	0.18
4.929	Phenol, 2-ethyl-	C ₈ H ₁₀ O	0.13
4.951	Cyclohexane, 2-propenyl-	C ₉ H ₁₆	0.06
5.016	Phenol, 2,3-dimethyl-	C ₈ H ₁₀ O	0.19
5.042	Cyclopentene, 1-pentyl-	C ₁₀ H ₁₈	0.06
5.064	8,10-Dodecadien-1-ol, (E,E)-	C ₁₂ H ₂₂ O	0.06
5.107	Cyclohexanol, 1-ethynyl-	C ₈ H ₁₂ O	0.19
5.133	Benzene, pentyl-	C ₁₁ H ₁₆	0.31
5.211	4-Methylphenyl acetone	C ₁₀ H ₁₂ O	0.09
5.246	Phenol, 3,5-dimethyl-	C ₈ H ₁₀ O	0.06
5.332	1-Dodecene	C ₁₂ H ₂₄	0.84
5.397	Dodecane	C ₁₂ H ₂₆	1.46
5.432	3-Dodecene, (Z)-	C ₁₀ H ₂₀	0.28
5.467	Phenol, 2,3,6-trimethyl-	C ₉ H ₁₂ O	0.06
5.506	2-Dodecene, (Z)-	C ₁₂ H ₂₄	0.17
5.584	Z-1,6-Undecadiene	C ₁₂ H ₂₀	0.07
5.606	Phenol, 2,3,5-trimethyl-	C ₉ H ₁₂ O	0.06
5.684	Phenol, 2-ethyl-4-methyl-	C ₉ H ₁₂ O	0.13
5.731	1-Tridecene	C ₁₃ H ₂₆	0.17
5.792	1,E-8,Z-10-Tridecatiene	C ₁₃ H ₂₂	0.12
5.818	p-Aminotoluene	C ₇ H ₉ N	0.05
5.840	2,4-Dodecadiene, (E,Z)-	C ₁₂ H ₂₂	0.07
5.883	Bicyclo[6.4.0]dodeca-9,11-diene	C ₁₂ H ₁₈	0.18
5.090	Phenol, 2-ethyl-4-methyl-	C ₉ H ₁₂ O	0.07
5.935	Benzene ethanol, .beta.-methyl-	C ₉ H ₁₂ O	0.14
6.004	Phenol, 2,3,4,6-tetramethyl-	C ₁₀ H ₁₄ O	0.12
6.056	1-Tridecene	C ₁₃ H ₂₆	1.59
6.117	Tridecane	C ₁₃ H ₂₈	2.97
6.143	3-Tridecene, (Z)-	C ₁₄ H ₂₈	0.24
6.217	2-Tridecene, (E)-	C ₁₄ H ₂₈	0.17
6.260	1H-Imidazole, 2-ethyl-	C ₅ H ₈ N ₂	0.08
6.455	Cyclopentane, (2-methylpropyl)-	C ₁₉ H ₁₈	0.33
6.503	Cyclopentene, 1-octyl-	C ₁₃ H ₂₄	0.21
6.642	1-Methyl-2-n-hexylbenzene	C ₁₃ H ₂₀	0.10
6.676	Cyclopentane, (2-methylpropyl)-	C ₉ H ₁₈	0.16
6.741	2-Tetradecene, (E)-	C ₁₄ H ₂₈	2.85

Time (min)	Name	Formula chemical	Area (%)
6.798	Tetradecane	C ₁₄ H ₃₀	4.62
6.819	3-Tetradecene, (Z)-	C ₁₄ H ₂₈	0.43
6.893	3-Tetradecene, (Z)-	C ₁₄ H ₂₈	0.27
6.941	Naphthalene, 1,6-dimethyl-	C ₁₂ H ₁₂	0.25
6.993	Cyclotetradecane	C ₁₄ H ₂₈	0.17
7.075	8-Hexadecyne	C ₁₆ H ₃₀	0.26
7.140	Cyclopentane, decyl-	C ₁₅ H ₃₀	1.08
7.179	Cyclopentene, 1-octyl-	C ₁₃ H ₂₄	0.48
7.275	Cyclohexene, 1-octyl-	C ₁₄ H ₂₆	0.69
7.353	Cyclopentadecane	C ₁₅ H ₃₀	1.44
7.383	1-Pentadecene	C ₁₅ H ₃₀	1.81
7.444	Pentadecane	C ₁₅ H ₃₂	9.24
7.491	1-Octadecyne	C ₁₈ H ₃₄	0.24
7.582	(1S)-(+)-Menthyl chloroformate	C ₁₁ H ₁₉ ClO ₂	0.85
7.643	Cyclohexane, (1-methylpropyl)-	C ₁₀ H ₂₀	0.47
7.726	Cyclohexene, 1,6-dimethyl-	C ₈ H ₁₄	0.33
7.795	n-Nonylcyclohexane	C ₁₅ H ₃₀	2.19
7.851	Cyclohexadecane	C ₁₆ H ₃₂	0.33
7.916	Cyclohexene, 1-nonyl-	C ₁₅ H ₂₈	2.33
7.955	Z-8-Hexadecene	C ₁₆ H ₃₂	1.56
7.994	Cetene	C ₁₆ H ₃₂	1.47
8.037	Hexadecane	C ₁₆ H ₃₄	2.36
8.059	Z-8-Hexadecene	C ₁₆ H ₃₂	0.51
8.116	Cyclopentane, (2-methylpropyl)-	C ₉ H ₁₈	0.41
8.189	Cyclopentene, 5-hexyl-3,3-dimethyl-	C ₁₃ H ₂₄	0.52
8.224	6-Methyl-bicyclo[4.2.0]octan-7-ol	C ₉ H ₁₆ O	0.37
8.259	Cyclodecanol	C ₁₀ H ₂₀ O	0.26
8.302	Trans-1-methyl-2-nonyl-cyclohexane	C ₁₀ H ₂₀	0.48
8.341	1-Methyl-2-methylenecyclohexane	C ₈ H ₁₄	0.36
8.441	Pentadec-7-ene, 7-bromomethyl-	C ₉ H ₃₁ Br	1.02
8.497	8-Heptadecene	C ₁₇ H ₃₄	2.15
8.528	8-Heptadecene	C ₁₇ H ₃₄	2.98
8.571	E-14-Hexadecenal	C ₁₆ H ₃₀ O	1.09
8.614	Heptadecane	C ₁₇ H ₃₆	3.12
8.636	E-14-Hexadecenal	C ₁₆ H ₃₀ O	1.19
8.705	8-Heptadecene	C ₁₇ H ₃₄	0.81
8.848	2-Methyl-Z-4-tetradecene	C ₁₅ H ₃₀	0.30
8.926	7-Octadecyne, 2-methyl-	C ₁₉ H ₃₆	0.21
8.952	Heptadecane, 2-methyl-	C ₁₈ H ₃₈	0.55
8.991	Cyclohexane, 2-propenyl-	C ₉ H ₁₆	0.72
9.039	5-Octadecene, (E)-	C ₁₈ H ₃₆	0.41
9.069	9-Octadecene, (E)-	C ₁₈ H ₃₆	0.71
9.087	9-Octadecene, (E)-	C ₁₈ H ₃₆	0.59
9.148	Octadecane	C ₁₈ H ₃₈	1.26
9.169	E-15-Heptadecenal	C ₁₇ H ₃₂ O	0.40
9.260	Cyclopentadecanone, 2-hydroxy-	C ₁₅ H ₂₈ O ₂	0.33
9.299	(R)-(-)-14-Methyl-8-hexadecyn-1-ol	C ₁₇ H ₃₂ O	0.24
9.395	7-Pentadecyne	C ₁₅ H ₂₈	0.22
9.473	Z,E-3,13-Octadecadien-1-ol	C ₁₈ H ₃₄ O	0.22
9.525	cis-11-Tetradecen-1-ol	C ₁₄ H ₂₈ O	0.37
9.559	1-Heneicosanol	C ₂₁ H ₄₄ O	0.22
9.585	9-Nonadecene	C ₁₉ H ₃₈	0.90
9.629	Z-5-Nonadecene	C ₁₉ H ₃₈	0.21
9.672	Hexadecane	C ₁₆ H ₃₄	0.68
9.702	2-Heptadecanone	C ₁₇ H ₃₄ O	2.69
9.772	1-Eicosene	C ₂₀ H ₄₀	0.15
9.806	Hexadecanoic acid, methyl ester	C ₁₇ H ₃₄ O ₂	0.18
9.963	13-Tetradecen-1-ol acetate	C ₁₆ H ₃₀ O ₂	0.44
10.045	1,19-Eicosadiene	C ₂₀ H ₃₈	0.20
10.084	Cyclopropanoethanal, 2-octyl-	C ₁₉ H ₃₆ O	0.46
10.171	Octadecan-4-one	C ₁₈ H ₃₆ O	1.14
10.348	7-Heptadecyne, 1-chloro-	C ₁₇ H ₃₁ Cl	0.11
10.405	Eicosane	C ₂₀ H ₄₂	0.17
10.578	Z,E-3,13-Octadecadien-1-ol	C ₁₈ H ₃₄ O	2.36
10.639	Octadecane	C ₁₈ H ₃₈	0.28
10.682	2-Nonadecanone	C ₁₉ H ₃₈ O	0.32

Time (min)	Name	Formula chemical	Area (%)
10.834	Oleic Acid	C ₁₈ H ₃₄ O	0.66
10.934	2-Dodecen-1-yl(-)succinic anhydride	C ₁₆ H ₂₆ O ₃	0.14
10.968	3,4-Octadiene, 7-methyl-	C ₉ H ₁₆	0.14
11.012	6-Octadecenoic acid	C ₁₈ H ₃₄ O ₂	0.37
11.094	Docosane	C ₂₂ H ₄₆	0.11
11.116	9-Octadecenoic acid, (E)-	C ₁₈ H ₃₄ O ₂	0.17
11.467	1-Tricosene	C ₂₃ H ₄₆	0.36
11.528	1-Chloroeicosane	C ₂₀ H ₄₁ Cl	0.09
11.571	.beta.-Piperidinopropiophenone	C ₁₄ H ₁₉ NO	0.08
11.887	Pyrrolidine, 1-(1-oxopentadecyl)-	C ₁₉ H ₃₇ NO	0.27
11.926	Benzene, 1-fluoro-4-methoxy-	C ₇ H ₇ FO	0.26
12.347	Eicosane	C ₂₀ H ₄₂	0.05
13.058	10-Nonadecanone	C ₁₉ H ₃₈ O	0.06
14.406	Cyclotrisiloxane, hexamethyl-	C ₆ H ₁₈ O ₃ Si ₃	0.10
14.432	Cyclotrisiloxane, hexamethyl-	C ₆ H ₁₈ O ₃ Si ₃	0.09
15.243	Silane, chlorodiethylheptyloxy-	C ₁₁ H ₂₅ ClOSi	0.09
16.396	13H-Dibenzo[a,i]carbazole	C ₂₀ H ₁₃ N	0.32

Figure 10 shows the concentration of CO₂, indicating that a significant fraction of oxygen from triglyceride fatty acid in palm oil was converted to CO₂ and short chain hydrocarbon molecules were generated. A possible reason for this phenomenon is that the higher temperature accelerated the thermal cracking and hence changing the long chain of hydrocarbon molecules to middle hydrocarbon and light hydrocarbon molecules [35-43]. Therefore light hydrocarbon molecules were thermally and catalytically cracked, converting them into gaseous product.

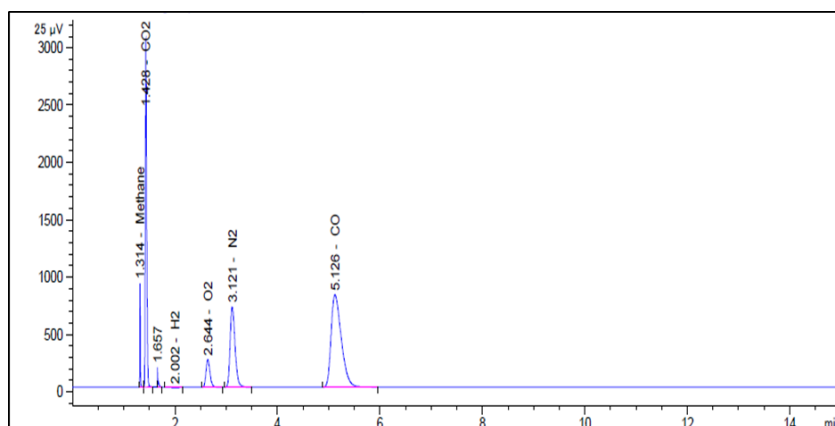


Figure 10. GC chromatograph of gas products from cracking of Palm oil from EFB on dolomite in continuous reactor

4. Conclusion

This research aimed to discover variables that significantly affect the catalytic cracking process of PEFB over dolomite in a continuous reactor and to find the optimum condition that will produce the maximum yield of organic liquid products (OLP) and diesel-like fraction. Using the 2^k factorial design, the researchers investigated the effects of reaction temperature, feed rate of palm oil, nitrogen gas flow rate and the amount of catalyst (v/v% by reactor volume) on the yield of OLP and diesel-like fraction, where the liquid products were obtained and analyzed by using distillation simulation gas chromatography and gas chromatograph mass-spectrometry to identify the structure of liquid fuels.

An analysis from a design-expert program indicated that the optimum conditions for the catalytic cracking of PEFB on dolomite in a continuous reactor were the following: a temperature of 460°C, feed rate of palm oil 8.96 mL/min, nitrogen gas flow rate of 50.04 mL/min, and the amount of catalyst 60% (v/v). These conditions led to the highest yield of diesel-like fraction of 66.12%wt and a liquid yield of 57.93%wt. It was found that basic catalyst gave a product with relatively low acid value. The results demonstrate that biofuel from catalytic cracking of PEFB has characteristics similar to those of petroleum fuels.

Acknowledgments

The authors wish to express their gratitude to Southern Palm (1978) Company Limited and Chulalongkorn University's Endowment Ratchadaphiseksomphot Fund for their financial support of this project.

References

- [1] Tani H, Hasegawa T, Shimouchi M, Asami K, Fujimoto K. Selective catalytic decarboxy-cracking of triglyceride to middle-distillate hydrocarbon. *Catalysis Today*, 2001; 164(1): 410-414.
- [2] Ulf S, Ricardo S, Rogério MV. Transesterification of vegetable oils: A review. *Journal of the Brazilian Chemical Society*, 1998; 9(1): 199-210.
- [3] Le TT, Kenj, O, Luu VB, Yasuaki M. Catalytic technologies for biodiesel fuel production and utilization of glycerol: A review. *Catalysts*, 2012; 2: 191-222.
- [4] Goyal G, Kuhn JN, Philippidis GP. Light alkene production by cracking *Picochlorum oculatum* microalgae using aluminosilicate catalysts. *Biomass and Bioenergy*, 2018; 108: 252-257.
- [5] Ch Luadthong, P Khemthong, W Nualpaeng, K Faungnawakij. Copper ferrite spinel oxide catalysts for palm oil methanolysis. *Applied Catalysis A: General*, 2016; 525: 2016, 68-75.
- [6] Heuchel M, Reinhardt F, Merdanoğlu N, Klemm E, Traa Y. Co-catalytic cracking of n-decane and 2-ethylphenol over a variety of deactivated zeolites for the conversion of fossil- and bio-based feeds in Co-FCC. *Microporous and Mesoporous Materials*, 2017; 2017: 59-68.
- [7] Alipour R, Esfahani M, Osmieri L, Specchia S, Yusup S, Tavasoli A, Zamaniyan A. H₂-rich syngas production through mixed residual biomass and HDPE waste via integrated catalytic gasification and tar cracking plus bio-char upgrading. *Chemical Engineering Journal*, 2017; 308: 578-587.
- [8] Venkateswarulu TC, Cherukuwada V, Kodali VP, John DB, Ranganaha Reddy A, Indira M, Venkatanarayana A. A renew on methods of transesterification of oils and fats in bio-deisel formation. *International Journal of Chemtech Research*, 2010; 6(4): 2568-2576.
- [9] Santillan-Jimenez E, Loe R, Garrett M, Morgan T, Crocker M. Effect of Cu promotion on cracking and methanation during the Ni-catalyzed deoxygenation of waste lipids and hemp seed oil to fuel-like hydrocarbons. *Catalysis Today*, 2018; 302: 261-271.
- [10] Huiyan Z, Rui X, He H, Gang X. Comparison of non-catalytic and catalytic fast pyrolysis of corncob in a fluidized bed reactor. *Bioresource Technology*, 2009; 100(3):1428-34.
- [11] Itthibenchapong V, Srifa A, Kaewmeesri R, Kidkhunthod P, Faungnawakij K. Deoxygenation of palm kernel oil to jet fuel-like hydrocarbons using Ni-MoS₂/γ-Al₂O₃ catalysts. *Energy Conversion and Management*, 2017; 134: 188-196.
- [12] Galeano JD, Mitchell DA, Krieger N. Biodiesel production by solvent-free ethanolysis of palm oil catalyzed by fermented solids containing lipases of *Burkholderia contaminans*. *Biochemical Engineering Journal*, 2017; 127: 77-86.
- [13] Jung YH, Park HM, Park Y-Ch, Park K, Kim KH. Efficacy of pretreating oil palm fronds with an acid-base mixture catalyst. *Bioresource Technology*, 2017; 236: 234-237.
- [14] Wheeldon I, Christopher P, Blanch H. Integration of heterogeneous and biochemical catalysis for production of fuels and chemicals from biomass. *Current Opinion in Biotechnology*, 2017; 45: 127-135.
- [15] Alzate CAC, Toro JCS, Peña ÁG. Fermentation, thermochemical and catalytic processes in the transformation of biomass through efficient biorefineries. *Catalysis Today*, 2018; 302: 61-72.
- [16] GY Chen, R Shan, B-B Yan, J-F Shi, S-Y Li, Ch-Y Liu. Remarkably enhancing the biodiesel yield from palm oil upon abalone shell-derived CaO catalysts treated by ethanol. *Fuel Processing Technology*, 2016; 143: 110-117.
- [17] Shahbaz M, Yusup S, Inayat A, Patrick DO, Ammar M. The influence of catalysts in biomass steam gasification and catalytic potential of coal bottom ash in biomass steam gasification: A review. *Renewable and Sustainable Energy Reviews*, 2017; 73: 468-476.
- [18] Sudiyani Y, Styarini D, Triwahyuni E, Sembiring KC, Aristiawan Y, Abimanyu H, Han MH. Utilization of biomass waste empty fruit bunch fiber of palm oil for bioethanol production using pilot – scale unit. *Energy Procedia*, 2013; 32: 31-38.
- [19] Somrat K, Kongkaew L. 2011. Renewable energy from palm oil empty fruit bunch. *Renewable Energy from Palm Oil Empty Fruit Bunch*, Renewable Energy - Trends and Applications, Dr. Majid Nayeripour (Ed.), ISBN: 978-953-307-939-4.
- [20] Boonyawan Y, Parncheewa U, Buppa P. Hydration-dehydration technique for property and activity improvement of calcined natural dolomite in heterogeneous biodiesel production: Structural transformation aspect. *Applied Catalysis A: General*, 2011; 395: 87-94.

- [21] Nongbe MC, Ekou T, Ekou L, Yao KB, Le Grogne E, Felpin F-X. Biodiesel production from palm oil using sulfonated graphene catalyst. *Renewable Energy*, 2017; 106: 135-141.
- [22] McIntosh RM, Sharp JH, Wilburn FW. The thermal decomposition of dolomite. *Thermochimica Acta*, 1990; 165: 281-296.
- [23] Shan R, Shi J, Yan B, Chen G, Yao J, Liu Ch. Transesterification of palm oil to fatty acids methyl ester using K_2CO_3 /palygorskite catalyst. *Energy Conversion and Management*, 2016; 116: 142-149.
- [24] Korkut I, Bayramoglu M. Ultrasound assisted biodiesel production in presence of dolomite catalyst. *Fuel*, 2016; 180: 624-629.
- [25] Rapagnà S, Gallucci K, Foscolo PU. Olivine, dolomite and ceramic filters in one vessel to produce clean gas from biomass. *Waste Management*, 2018; 71: 792-800.
- [26] Yoosuk B, Udomsap P, Puttasawat B. Hydration–dehydration technique for property and activity improvement of calcined natural dolomite in heterogeneous biodiesel production: Structural transformation aspect. *Applied Catalysis A: General*, 2011; 395(1–2): 87-94
- [27] Quitete CPB, Souza MMVM. Application of Brazilian dolomites and mixed oxides as catalysts in tar removal system. *Applied Catalysis A: General*, 2017; 536: 1-8.
- [28] Qian H, Kai W, Hongde X. A novel perspective of dolomite decomposition: Elementary reactions analysis by thermogravimetric mass spectrometry. *Thermochimica Acta*. 2019; 676: 47-51.
- [29] Charusiri W, Vitidsant T. Upgrading bio-oil produced from the catalytic pyrolysis of sugarcane (*Saccharum officinarum* L) straw using calcined dolomite. *Sustainable Chemistry and Pharmacy*, 2017; 6: 114-123.
- [30] Otsuka T. Recent studies on the decomposition of the dolomite group by thermal analysis. *Thermochimica Acta*, 1986; 100: 69-80.
- [31] Pinthong Ch, Phoopraintra P, Chantiwas R, Pongtharangkul T, Chenprakhon P, Chaiyen P. Green and sustainable biocatalytic production of 3,4,5-trihydroxycinnamic acid from palm oil mill effluent. *Process Biochemistry*, 2017; 63: 122-129.
- [32] da Conceição LRV, Carneiro LM, Rivaldi JD, de Castro HF. Solid acid as catalyst for biodiesel production via simultaneous esterification and transesterification of macaw palm oil. *Industrial Crops and Products*, 2017; 89: 416-424.
- [33] Wheeldon I, Christopher P, Blanch H. Integration of heterogeneous and biochemical catalysis for production of fuels and chemicals from biomass. *Current Opinion in Biotechnology*, 2017; 45: 127-135.
- [34] Yang H, Chen Zh, Chen W, Chen Y, Wang X, Chen H. Role of porous structure and active O-containing groups of activated biochar catalyst during biomass catalytic pyrolysis. 2020: 210: 118646.
- [35] Ivan-Tan ChT, Islam A, Yunus R, Taufiq-Yap YH. Screening of solid base catalysts on palm oil based biolubricant synthesis. *Journal of Cleaner Production*, 2017; 48: 441-451.
- [36] Poosumas J, Ngaosuwan K, Quitain AT, Assabumrungrat S. Role of ultrasonic irradiation on transesterification of palm oil using calcium oxide as a solid base catalyst. *Energy Conversion and Management*, 2016; 120: 62-70.
- [37] Zhang B, Zhang L, Yang Zh, He Zh. An experiment study of biomass steam gasification over NiO/Dolomite for hydrogen-rich gas production. *International Journal of Hydrogen Energy*, 2017; 42: 76-85.
- [38] Boot-Handford ME, Virmond E, Florin NH, Kandiyoti R, Fennell PS. Simple pyrolysis experiments for the preliminary assessment of biomass feedstocks and low-cost tar cracking catalysts for downdraft gasification applications. *Biomass and Bioenergy*, 2018;108: 398-414.
- [39] Kannaiyan S, Madhavan VR, Rajagopal S, Jayabalan A. An experimental analysis on tar cracking using nano structured Ni-Co/Si-P catalyst in a biomass gasifier-based power generating system. *Applied Thermal Engineering*, 2016; 97: 13-21.
- [40] Promdee K, Vitidsant T. Preparation of Biofuel by Pyrolysis of PlantMatter in a Continuous Reactor. *Theoretical and Experimental Chemistry*, 2013; 49: 126 – 129.
- [41] Khuenkao N, MacQueen B, Onsree T, Daiya S, Tippayawong N, Lauterbach J. Bio-oils from vacuum ablative pyrolysis of torrefied tobacco residues. *RSC Advances.*, 2020; 10: 34986-34995.
- [42] Promdee K, Vitidsant T. Bio-oil synthesis by pyrolysis of Cogongrass (*Imperata cylindrica*). *Chemistry and Technology of Fuels and Oils*, 2013; 49: 287 – 292.
- [43] Auersvald M, Macek T, Schulzke T, Staš M, Šimáček P. Influence of biomass type on the composition of bio-oils from ablative fast pyrolysis. *Journal of Analytical and Applied Pyrolysis*, 2020; 150: 104838.

To whom correspondence should be addressed: Dr. Tharapong Vitidsant and Dr. Kittiphop Promdee, Center of fuels and Energy from Biomass, Chulalongkorn University, Saraburi 18110, Thailand, E-mail: nuumensci@gmail.com